



A spectroscopic and structural study on the solvent-promoted stereospecific self-assembly of new Porphyrin-Bile Salt conjugates

Valeria D'Annibale ^{a,b}, Luca Piccirillo ^{a,b}, Beatrice Pacini ^a, Simona Sennato ^c, Claudia Marconi ^{a,b}, Alessandra Del Giudice ^a, Maria Chiara di Gregorio ^a, Karin Schillén ^d, Marco D'Abramo ^a, Andrea D'Annibale ^{a,*}, Donato Monti ^{a,*}, Luciano Galantini ^{a,*}

^a Department of Chemistry, Sapienza University of Rome, P.le A. Moro, 5, Rome, 00185, Italy

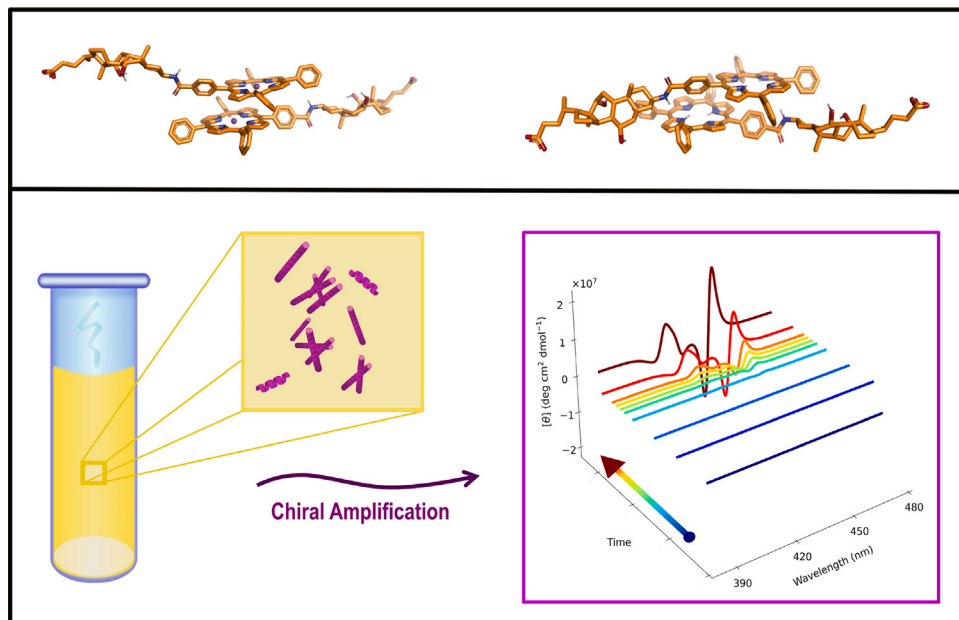
^b Department of Basic and Applied Sciences for Engineering, Sapienza University of Rome, P.le A. Moro, 5, Rome, 00185, Italy

^c Institute of Complex Systems (ISC-CNR) and Department of Physics, Sapienza University of Rome, P.le A. Moro, 5, Rome, 00185, Italy

^d Division of Physical Chemistry, Department of Chemistry, Lund University, P.O. Box 124, Lund, SE-22100, Sweden



GRAPHICAL ABSTRACT



ARTICLE INFO

Keywords:

Bile salts
Chirality
Porphyrin aggregates
Supramolecular chemistry

ABSTRACT

The chiral bile salt sodium cholate has been covalently linked to tetra-aryl-porphyrins, conferring them an extrinsic chirality and obtaining new molecules with high tendency to aggregate in solution. The chirality transfer from the molecular to the nano- and meso-scale has been investigated by promoting the self-assembly of the conjugates balancing the ratio of aqueous/organic solvent mixtures and allowing a fine control of the dimensions and morphology of the final supramolecular architectures. The shift from elongated structures with helical ribbon features to monodisperse tubules or from tightly packed rolled sheets to wrapped scrolls

* Corresponding author.

E-mail addresses: andrea.dannibale@uniroma1.it (A. D'Annibale), donato.monti@uniroma1.it (D. Monti), luciano.galantini@uniroma1.it (L. Galantini).

was enabled by changing the solvent composition, with the possibility of forming tubular structures with a hollow cavity. From UV-Vis and Circular Dichroism (CD) spectroscopy the ability to self-assemble into J-type aggregates with a strong induction of supramolecular chirality was revealed, shedding light on a two-step process, with a fast monomer nucleation followed by a slow second step of further stereospecific chiral evolution. The results as a whole promote the new porphyrin-cholate conjugates as promising smart and easily tunable chiral materials for the design of stereoselective sensing devices.

1. Introduction

The concept of *chirality* is one of the most important issue in chemistry being strictly related to the emergence of homochirality in life. This is because a large variety of biological compounds (*i.e.* DNA and RNA, amino acids and proteins, sugars) exists, almost exclusively, in a specific one of the many possible stereoisomers [1–5]. Therefore, chirality is fundamental for the interaction with biological environments, carefully considered in fields such as chemical recognition and sensing, drug-delivery, catalysis and widely investigated within *bio-inspired* material sciences [6–12]. Upon self-assembly, chirality is efficiently transferred and amplified, from small molecules to ordered and well organized supramolecular chiral macro-structures [6, 13]. Such supramolecular architectures enable the realization of smart materials, resembling the complexity of natural molecular machineries [14], where chirality is commonly expressed at every level [15]. Porphyrins, are unique and versatile building blocks for supramolecular organization [16]. Thanks to their aromatic platform and the possibility of easily tuning their properties by different functionalization or by changing the metal ion inside the core [17–19], they are particularly suitable to transfer the chirality from a molecular to a supramolecular level [10]. As natural chromophores they are optimal elements for the preparation of sensing materials for chiral recognition [20–22]. Chirality-transfer to new self-assembled structures can be induced by the presence of chiral peripheral groups on the porphyrinic macrocycle, as well as the interaction of achiral porphyrins with a chirality-inductor not covalently linked (*i.e.* polymeric templates or chiral surfactants [9]). For this reason, porphyrins are considered as chiral probes to obtain information on the chirality of a system [13], and result ideal molecules for deposition of sensing films [22].

A further advantage of introducing porphyrins into the system is that they are long-range interacting chromophores [23], able to reveal exciton coupling up to tens of Å, when an interaction between electric transition dipole moments of the single units takes place [23,24]. In particular, tetra-aryl-porphyrins exhibit relevant optical properties, that are generally exploited as circular dichroism (CD) reporters for detecting the chirality of organized supramolecular aggregates and for structural analysis [25]. Depending on the selected operative conditions, different types of porphyrins aggregates can be induced. Two limiting cases can be recognized, either H- or J-type aggregates, with the monomeric units stacked *face-to-face* or *edge-to-edge* respectively [16]. The latter type of structures, firstly described by Scheibe and Jolley [11,26,27], is often found in dye aggregates. They exhibit a red-shifted and hypochromic peak at the maximum wavelength in the absorption spectrum, with a splitting of the Soret band due to the exciton coupling of the transition dipole moments [16,26]. Aggregation of porphyrins is generally related to hydrophobic effects, as well as electrostatic and $\pi-\pi$ interactions between monomers that cooperatively self-assemble in organized structures. Hydrogen bonds, can also play a crucial stabilizing role, especially in aqueous systems [28].

Chiral surfactants have shown to be relevant chiral effectors in controlling the chiroptical properties of the porphyrin aggregates, by means of electrostatic interactions and hydrophobic effects. Especially the last ones, are considered as the driving force that efficiently determines the aggregate formation and thus the chirality transfer [13, 29]. The aggregation behaviour and the ability to transfer the chiral information of surfactants are strongly dependent on their molecular

structure. Due to self-assembly, the chiral recognition may happen also far from the stereogenic centres present in the single surfactant molecules, thereby showing a specific chirality, proper of the whole self-assembled structures [30]. Furthermore, the use of surfactants in aqueous media could have the relevant task of simulating artificial biological-like architectures (*i.e.* enzymes or antibodies) or providing drug-delivery systems (*i.e.* micelles, liposomes or tubular structures). Encapsulation of a chromophore in surfactant aggregates, with high biocompatibility and low toxicity [19,31], can be used in photodynamic therapy as anticancer or antibacterial drugs [32–36].

Bile salts (BSs), the anionic salts of bile acids, are a particular class of chiral biological surfactants. They are characterized by a rigid amphiphilic steroidal skeleton of four condensed rings [37] that confers them many physiological roles, such as antibiotic activity, detergent properties, regulation function and membrane permeation ability [37–39]. Their rigid amphiphilic structure enables them to self-assemble into aggregates with unconventional morphology, according to a complex, sometimes considered stepwise, self-assembly process [38]. Owing to their self-assembling behaviour BSs constitute inexpensive components for the preparation of specific materials. In particular, they can be used in the mixed assembly with organic dyes, by means of non-covalent interactions [38] or to pack into ordered supramolecular nanotubes and helices [40–43], with relevant application potential. Supramolecular association of BS and polyamines can be used to prepare oligomeric non covalent antimicrobials [44] as alternative to the conventional covalent versions [45] and in general the bile acid unit has been widely exploited to develop novel antimicrobials due to the features of biocompatibility and the ability of penetrating the bacterial membranes, mimicking the facial amphiphilic structures of antimicrobial peptides (AMPs) [46,47]. BSs can also be used as starting material in the synthesis of new BS derivatives by, *e.g.*, exploiting the functionalization of the C3 steroidal carbon atom, as already reported in literature for amino acidic or sugar derivatives [48–51] or for positively/negatively charged hydrophobic derivatives, functionalized with aromatic groups, recently exploited in the fabrication of novel supra-colloidal architectures [52,53].

In this context, starting from the last decades, with the aim of enhancing the chirality-transfer of porphyrins to a supramolecular level, many attempts have been carried out to synthesize new derivatives, to study their properties and to understand and optimize their supramolecular self-assembly. Generally, in absence of a peripheral chiral molecular group or without a chiral template or inductor, the aggregation process for achiral porphyrin macrocycles does not lead to a specific supramolecular chirality [54,55]. Recent studies on the aggregation behaviour of chiral proline-porphyrin derivatives in aqueous solution [9,10,56–60] revealed an important tendency of these systems to form supramolecular aggregates with intense chiroptical properties. These results set the basis for the realization of stereoselective porphyrin-based solid films as sensible material in quartz microbalance sensor devices, widely known as the *electronic nose* [61]. In the same way, great efforts are directed towards the functionalization of porphyrins with glycosylated [62], steroidal or glucosylated-steroidal moieties [63,64], with the aim of introducing elements of chirality as well as an amphiphilic character on the porphyrinic macrocycle. The application of such structures spans from anion receptors for nitrogen-based organic ligands, to molecular recognition, to drug-delivery systems, with an increasing attention on their behaviour in aqueous physiological conditions [11,65,66]. Various molecular structures of porphyrin-steroidal derivatives have been reported in the

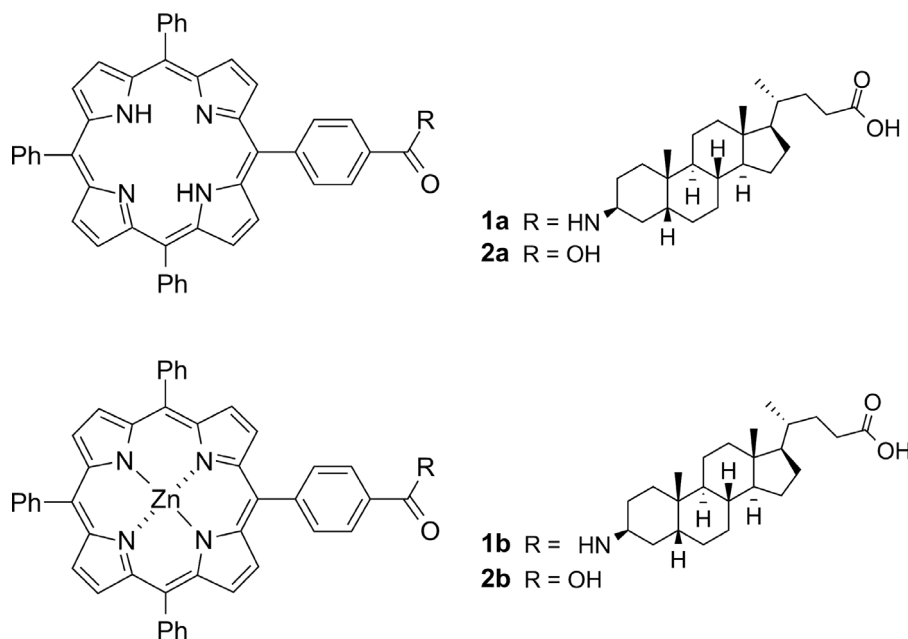


Fig. 1. Molecular structures of porphyrin-bile acid derivatives **1a** and **1b**.

literature, that differ from each other for the position of the functionalization on the porphyrinic skeleton and in the linking bridge between the two units, *i.e.* aliphatic, ester or amidic bridge and with different application targets [65,67–73].

Properly designed porphyrin derivatives may show a pivotal role also in photothermal and photodynamic therapy [74,75], exploiting as well the ability to self-organize in aggregates or to be delivered as encapsulated monomer drug, according to the structural and chemical features of the conjugated unit.

Within this scenario, in our work we carried out the synthesis of the new porphyrin-bile acid conjugates, **1a** and **1b**, from both the commercial 5-(4-carboxyphenyl)-10,15,20-(triphenyl)porphyrin **2a** and its Zinc(II) analogue **2b**. The structure of compounds **1a** and **1b**, in which the macrocycle and steroid moieties are covalently linked through an amidic bond in the C3 position of a cholic acid moiety, are shown in Fig. 1. We conducted a detailed study on the self-assembly of the two new porphyrins in the form of deprotonated bile salts (porphyrin-BS) and we will refer to them in the text as **1-H₂** (from **1a**) and **1-Zn** (from **1b**). The aim was to assess whether the covalently linked extrinsic chiral effector bile salt would efficiently transfer chirality to the aggregates in the self-assembly process.

Here, we defined the best conditions for inducing an efficient aggregation process in water/organic media (*i.e.* water/ethanol or water/acetonitrile mixtures). Tubular nano- and meso-aggregates were obtained upon self-assembly with a specific induced supramolecular chirality. The aggregates result particularly promising materials for the construction of stereoselective sensing devices, in the light of the potentiality of hollow chiral nanotubes for an enantioselective inclusion of guests [76,77]. In addition, we interestingly observed that a control over the tightness of packing and levels of organization, was achievable by regulating the stoichiometry of the solvent mixture and by properly choosing the free base or the Zn(II) form of the derivatives.

2. Material and methods

Synthesis of porphyrin-BS conjugates

Steroidal-porphyrin derivatives were synthesized according to the pathway reported in Scheme 1, that involves the conversion of the hydroxy group in C3 position of the cholic unit **3** in a primary amino

group (compound **7**), undergoing the coupling reaction with the (4-carboxyphenyl)-10,15,20-(triphenyl)porphyrin **2a,b**, to afford the amides **8a,b**. The subsequent hydrolysis of the steroid ester moieties of these latter compounds provides the expected derivatives **1a,b**. The synthetic scheme was defined starting from protocols previously described in literature [78–81].

Noteworthy, along the synthetic path, an inversion of the steroid C3 configuration occurs, leading only to the 3-(β)-azido-derivative **6**, thus stereoselectively affording in the end compounds **1a,b**. A more detailed description of the synthesis procedure and the employed materials are reported in the supporting information (section 1).

Sample preparation

Equimolar concentration (30 mM) of carbonate-bicarbonate (at total concentration of 60 mM) were dissolved in Milli-Q grade distilled water, to obtain a pH 10.0 buffer. The alkaline pH was chosen to guarantee a better solubilization of the porphyrin in an aqueous environment with complete deprotonation of the carboxylic groups and to control the ionic strength for promoting efficient aggregation [62].

Porphyrin stock solutions with a concentration of 10^{-4} M were prepared in acetonitrile (*i.e.* non aggregative conditions) and used after filtering with Millipore Millex-GV hydrophilic PVDF filters (0.22 μ m pore size). Acetonitrile and water buffer were filtered as well, in order to reduce the presence of dust and unidentified traces of biological contaminants, able to trigger a symmetry breaking that could alter the aggregation behaviour reproducibility [55].

Aggregates were obtained in aqueous buffer/acetonitrile media at v/v ratios of 7/3 and 8/2, at a porphyrin concentration of 10^{-5} M, achieved by a proper addition of acetonitrile and aqueous buffer to an aliquot of stock solution sample. The aggregation process was carried out by strictly following the established porphyrin – first protocol [9]. A proper amount of water (the *solvophobic* medium) was slowly added to a volume of acetonitrile porphyrin solution (the *solvophilic* medium), driving the aggregation by hydrophobic effects [11]. After the water addition, a brief sonication (15–20 s) in ultrasound bath was applied, in order to homogenize the initially formed aggregation nuclei of the assembling molecular architecture [82].

Aggregates samples were all prepared at the temperature of 298 K.

Acetonitrile (\geq 99.8%), Na₂CO₃ (\geq 99.5%) and NaHCO₃ (\geq 99.8%) were purchased from Carlo Erba and used for sample preparation.

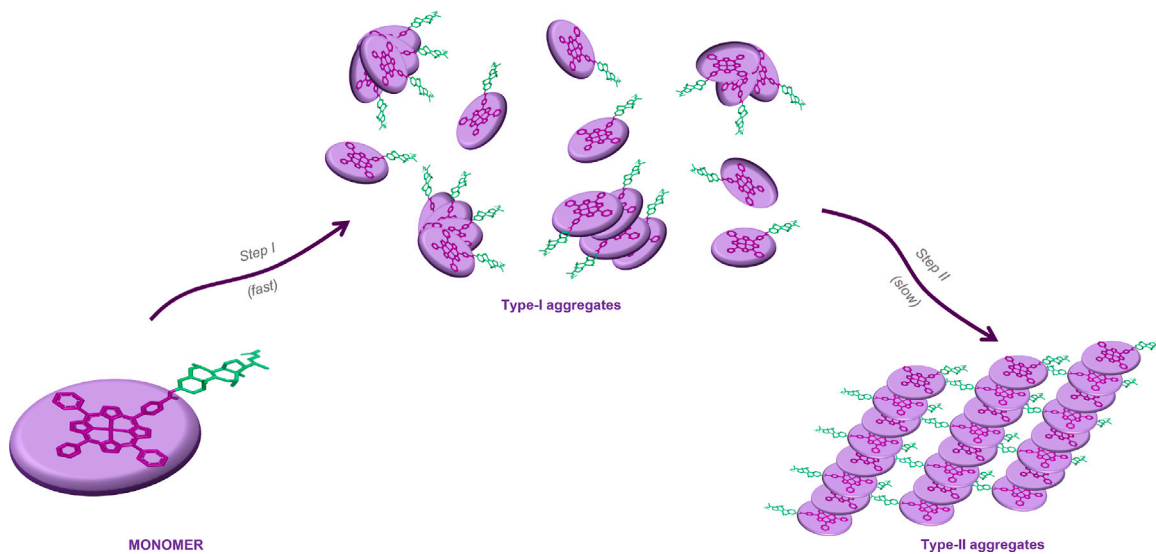
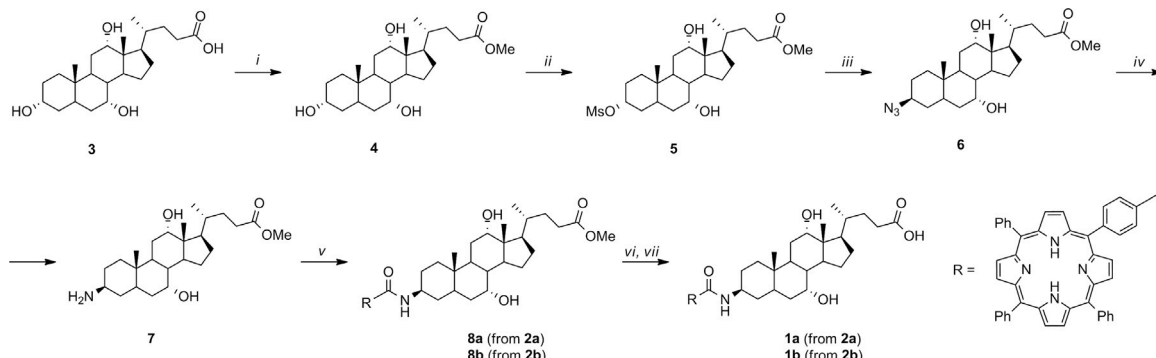


Fig. 2. A schematic representation of the aggregation path, that proceeds from the monomeric state to an initial fast organization in proto-aggregates (Type-I), driven predominantly by hydrophobic effects between porphyrin rings, converging then to a slower structuring of well organized and stereospecific final architectures (Type-II).



Scheme 1. Synthetic pathway to **1a,b**. (i) MeOH, H_2SO_4 (cat), 80 °C, 3 h (97%); (ii) MsCl , Et_3N , CH_2Cl_2 , r.t., 8 h; (iii) NaN_3 , DMF, 80 °C, 24 h (70%, 2 steps); (iv) H_2 , Pd/C 10%, MeOH, r.t., 24 h (70%); (v) **2a** (or **2b**), DCC, HOBr, Et_3N , CH_2Cl_2 , 35 °C, 72 h (40%) (for **1b**, 53%); (vi) NaOH , $\text{THF}/\text{H}_2\text{O}$, 40 °C, 24 h, then (vii) Citric acid, H_2O , r.t., 1 h (90% for **1a**, 66% for **1b**, 2 steps).

The starting not functionalized 5-(4-carboxyphenyl)-10,15,20-(triphenyl)porphyrins were purchased from PorphyChem.

UV-Vis and CD spectroscopy

UV-Vis absorption spectra were recorded with a Jasco V-530 spectrophotometer, using a scanning speed of 100 nm/min and a band width of 2 nm, on a single acquisition. CD spectra were recorded with a Jasco J-715 spectropolarimeter, using a scanning speed of 100 nm/min and a band width of 1 nm, on a single acquisition. Measurements were conducted always at 298 ± 0.5 K (thermostated with a Peltier unit), using quartz or optical glass cuvettes. The effect of a linear dichroism was excluded, by checking CD spectra reproducibility at different cuvette distances with respect to detector.

Dynamic Light Scattering (DLS)

DLS measurements were performed at 298 K with a Zetasizer Nano ZS instrument, from Malvern Instruments (now part of Malvern Panalytical), Malvern, UK, equipped with a 4 mW He-Ne laser (at 632.8 nm). The auto-correlation functions of the scattered intensity were measured at a scattering angle of 173°.

Atomic Force Microscopy (AFM)

AFM sample preparation have been performed by depositing a drop of 10 μL and letting it to dry overnight on mica supports, then washed with Milli-Q water, to remove the sample excess and the buffer salt. Measurements were conducted using a Dimension Icon (Bruker AXS), at room temperature and under ambient pressure, in Tapping Mode. RTESP-300 (Bruker) probes (nominal radius of curvature 10 nm) have been used, whose cantilever has a nominal spring constant of 40 N/m and a length of 125 μm . Gwiddion software was adopted for image processing and background subtraction on height sensor channel data was performed with line-by-line or three-point data levelling.

Scanning Electron Microscopy (SEM)

SEM measurements were performed with a HR-FESEM AURIGA ZEISS instrument, operating at 1.5 kV voltage. Images were collected in secondary electron mode, by means of an Everhart Thornley Detector. Samples were prepared dropping few microlitres of the solution on silicon plates, letting it to absorb overnight, and lastly washing with Milli-Q water to remove the excess sample and the salt from the buffer solution. Deposited and washed samples were left to air dry for one hour before measuring.

Computational details

Molecular optimization of the dimer structure for **1-Zn** and **1-H₂** was realized by DFT calculation using wB97XD as long-range interactions corrected functional [83]. As basis set, 6-31G was used for the atomic description of H atoms, 6-31G* for C, N, O and 6-31+G* for Zn, in the specific case of the Zn-derivative. The solvent environment was implicitly considered as a water continuum dielectric, by means of the Polarizable Continuum Model (PCM) [84]. All the calculations were performed by Gaussian 16 software [85].

Optimized geometries of the porphyrin dimers were reported in section 10 of the supporting material (Fig. S11–S12).

Kinetic studies

Generally, the porphyrin aggregation kinetics undergoes a two-steps evolution in time, with a fast formation of aspecific proto-aggregates (step I, leading to Type I aggregates), followed by a specific and slower auto-catalytic growth towards bigger structures (step II, leading to Type II aggregates), as reported in Fig. 2. Following the kinetic of the auto-catalytic step (step II) requires an unconventional fitting equation for the description of the evolution in time of the assembly growth. Using the equation formerly defined by Pasternack et al. [86,87], we described in our analysis the case of an auto-catalyzed formation of organized suprastructures, with a time-dependent rate constant.

Eq. (1) [87] is a reduced form of a more general equation [86], derived by Pasternack in the limiting case of $m \rightarrow 1$ (where m is the number of *critical nuclei* able to catalyze the assembly formation), accounting for an initial lag phase, evolving in an auto-catalyzed aggregates formation and can be written as:

$$Abs(t) = Abs(t_{\infty}) + [Abs(t_0) - Abs(t_{\infty})] \times e^{-\frac{(k_f t)^{(n+1)}}{n+1}} \quad (1)$$

Where $Abs(t)$ is the absorbance at time t ; $Abs(t_0)$ and $Abs(t_{\infty})$ are the absorbance values at time 0 and at equilibrium, respectively; k_f is the formation constant and n is the growth factor. Spectral trends that follow this equation have been commonly ascribed to the formation of complex fractal or tubular structures [88,89].

3. Results and discussion

3.1. Aggregation studies: the effect of the solvent

Both derivatives were insoluble in water due to their hydrophobicity. Therefore, mixtures of water and a less polar co-solvent were used to solubilize them and characterize their self-assembly. Ethanol was initially used, due to its wide application in tuning the aggregation of porphyrins in solution [9,57,58].

However, preliminary measurements demonstrated that in the case of the metallo-derivative, the presence of ethanol as co-solvent drastically inhibits the self-assembly process, which is observed to occur with extremely long time. The effect of ethanol to detrimentally affect the aggregation process is likely due to the strong coordination ability towards the Zn(II) ion of the porphyrinic core, acting as a Lewis base, thus hampering an efficient self-assembly of the tetra-pyrrolic platform, as reported in the literature [58]. Based on this hypothesis, the Gutmann's donor number (DN) – a parameter that quantifies the Lewis basicity of a solvent in terms of its cation affinity [90–93] – was used as guideline and acetonitrile was selected as alternative organic co-solvent, owing to its lower DN (14.1 kcal/mol, instead of 19.2 kcal/mol featured by ethanol) [90] and its capability to properly solubilize the porphyrin-BS derivatives.

For the analysis of the UV-Vis absorption spectra, the extinction coefficients for the maximum absorption of the Soret band in pure acetonitrile (*i.e.* non-aggregative conditions) for **1-Zn** (λ_{max} at 423 nm) and **1-H₂** (λ_{max} at 421.5 nm) were estimated and reported in SI (section 2, Fig. S2–S3 and Table S1).

3.2. Aggregation kinetics in buffer/acetonitrile mixtures

In order to shed light on the self-assembly behaviour of the derivatives, aggregation kinetics were analysed for **1-Zn** and **1-H₂**. In a pure organic solvent porphyrins are in their monomeric state. By increasing the volume percentage of water over 50%, the Soret band starts broadening with a general hypochromic trend, indicating the formation of aggregated structures, driven by hydrophobic effects [58]. In our study, we considered water buffered with carbonate/bicarbonate and volume ratios of buffer aqueous solution and acetonitrile organic solvent of 7/3 and 8/2. The role of carbonate/bicarbonate buffer was already demonstrated to play a relevant role in keeping the BS and derivatives carboxylic function deprotonated and guaranteeing optimal aggregation conditions [37,48,49,94]. The solvent composition was found to be a relevant factor in the kinetic behaviour and for tuning the final aggregate shape and morphology, as evidenced by SEM and AFM microscopies. UV-Vis and CD spectroscopies were here used to elucidate the kinetic behaviour by following the spectral evolution in time.

The aggregation processes follow a clear two-step behaviour (see the scheme reported in Fig. 2). In the initial fast step (step I), a monomer nucleation provides structures featuring a low degree of specificity (Type-I aggregates). A broadening of the maximum absorption peak is observed at this stage, with a general hypochromic effect. The primary aggregation nuclei are relevant for determining the enantiomeric excess, leading to the emergence of a growth-direction for the aggregates. This early stage is completed during the time of preparation of the solution and it is followed by a second slower step of further growth and rearrangement of the supramolecular chiral organization (step II), featuring high specificity and high degree of supramolecular chirality (Type-II aggregates) [54,57,95]. The kinetic of this second auto-catalytic step was followed by conventional UV-Vis and CD spectroscopy, and the fitting of intensity variations resulted in perfect agreement with the kinetic rate law defined in Eq. (1).

As a general trend, at 30%_{vol} of acetonitrile in the solvent mixture, faster processes have been found compared to those observed when a 20%_{vol} of organic solvent is present. Furthermore, the metal ion inside the porphyrinic core strongly affects the aggregates formation [58], reducing the overall aggregation rates, due to the solvent coordination. An evidence of this is that the Zn(II)-porphyrin (**1-Zn**, deprotonated form of molecule **1b** in Fig. 1), in both solvent conditions, showed a much slower aggregation kinetics in comparison to the free base porphyrin (**1-H₂**, deprotonated form of molecule **1a** in Fig. 1) for the aggregate formation. As shown in Table 1, this is reflected in the values of the kinetic constant, the highest being when the free base porphyrin is considered and with a 30%_{vol} of acetonitrile in the solvent mixture. From the first rapid and aspecific nucleation, the broadening of the Soret band at around 420 nm was detected, meaning the formation of poorly structurally coherent proto-aggregates that do not result in any supramolecular chirality, as demonstrated by lack or negligible CD bands (*vide infra*) in the 350–550 nm region of the spectrum. The second slower step resulted in remarkable changes of the UV-Vis spectroscopic pattern, with the arise of a red-shifted Soret band, with typical exciton splitting and the decrease of the monomer absorption. The bathochromic shift and the coupled Soret band of the final suprastructures, with a general hypochromic effect, are a strong indication of the formation of complex architectures with local J-type packing [89,96]. Moreover, the formed structures feature, in all cases, intense supramolecular chirality, as a consequence of a highly efficient reading-out and amplification of the stereochemical information stored on the periphery of the tetra-pyrrolic macrocycles. The chirality transfer along the growth of the aggregates is revealed by the high CD intensities reached at the end of the process. All the spectroscopic results were reported in Figs. 3 and 4 a-d, for **1-Zn** and **1-H₂**, respectively. These results are well reproducible with peculiar complex spectral patterns, composed of multiple bisignated bands. Noteworthy,

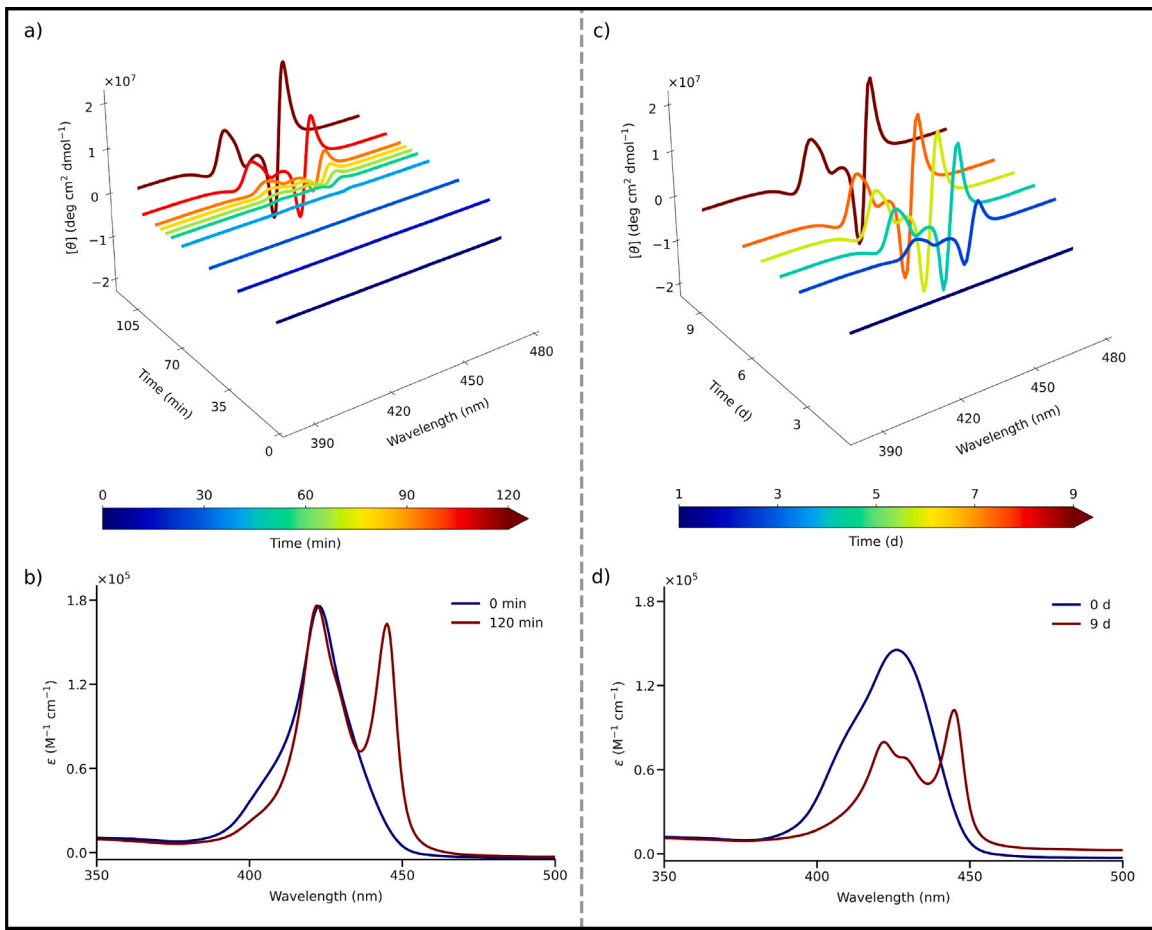


Fig. 3. (a) CD and (b) UV-Vis signal evolution in the time of few hours for **1-Zn** at 30%_{vol} of acetonitrile; (c) CD and (d) UV-Vis signal evolution in the time of few days for **1-Zn** at 20%_{vol} of acetonitrile. The colour-bar, from blue to red, designs the evolution in time from the first moments of the aggregation to reaching the maximum growth at equilibrium.

the most intense band, located in the red region of the spectra, show a +/- sign, likely indicating a local clockwise arrangement (P-type) of the aromatic platforms. In both the solvent conditions used (30 and 20%_{vol} of acetonitrile) and for both the conjugates, the UV-Vis absorption spectrum shows a splitted signal, typical of rod-shaped aggregates, with linear oscillators polarized along both a short and a long axis, as already reported by Kobayashi and Balaban groups [89,96]. In Table S2 of the supporting material, CD maxima and minima intensities were reported in a general overview of the results obtained, while in Table S3, the kinetic parameters for all the sets of experiments were reported (section 3 of SI).

In Fig. 5, the time evolution of CD maximum peaks was reported, clearly underlying the different trends between the two porphyrins (with or without the Zn ion) and between the solvent ratios used. The CD maxima were plotted *vs* time (minutes) and fitted with Eq. (1), showing a sigmoidal evolution in each condition.

3.2.1. Aggregation studies of **1-Zn** derivative

For the metallated derivative, at 30%_{vol} of acetonitrile in the aqueous medium, the second auto-catalytic step is completed within the time of few hours, with the shift of the Soret band up to 445 nm, as reported in Fig. 3, b. The evolution of the UV-Vis spectrum proceeds in accordance with the arise of a CD signal (Fig. 3, a), which demonstrates the coherent growth of the chiral aggregate [96]. Conversely, at 20%_{vol} of acetonitrile (*i.e.* in an aqueous richer medium), this second step achieves the completion in a longer time, of about ten days. Generally, the slower evolution into the final self-assembled structure is related to a more specific organization of the monomers into supramolecular

architectures. However, the CD spectral features, in terms of spectral pattern and intensities, are similar for both the solvent compositions, reaching theta molar intensities in the order of 10⁷ deg × cm² × dmol⁻¹, the largest values being centred at about 445 nm, in correspondence to the absorbance maximum of the J aggregates band.

In particular, when a 30%_{vol} of acetonitrile is considered, the mean value of the formation constant, k_f , evaluated on a set of experiments, was of $(1.6 \pm 0.3) \times 10^{-2}$ min⁻¹, while the value of n , describing the exponential growth of the aggregates as a power of time, was of 12 ± 1 . Differently, in the case of 20%_{vol} of acetonitrile, the kinetic parameters remarkably change, with an estimated k_f reduced by two order of magnitude - $(1.2 \pm 0.2) \times 10^{-4}$ min⁻¹ - and a growth factor n of 4 ± 2 . The decrease of both these parameters (formation constant and n) indicates the strong effect of small composition variation in the solvent media, likely due to the solvent coordination to the central ion of the porphyrin platforms.

3.2.2. Aggregation studies of **1-H₂** derivative

In the case of **1-H₂**, the Soret band, in the early stages of aggregates formation, appears as a broadened peak at around 421 nm, in both the solvent compositions of 30 and 20%_{vol} of acetonitrile (Fig. 4, b-d). The kinetics, for both the mixtures, is faster than that of the above-mentioned Zn(II) counterpart, corroborating the formulated hypothesis of the involvement of solvent coordination to the porphyrinic metal centre. Here, the difference in solvent composition more relevantly affects the transmission of the aggregates chiral features. With a 30%_{vol} of acetonitrile, a fast aggregation occurs, which is completed in about 30 min. At the end of the process, the absorption maximum is relevantly

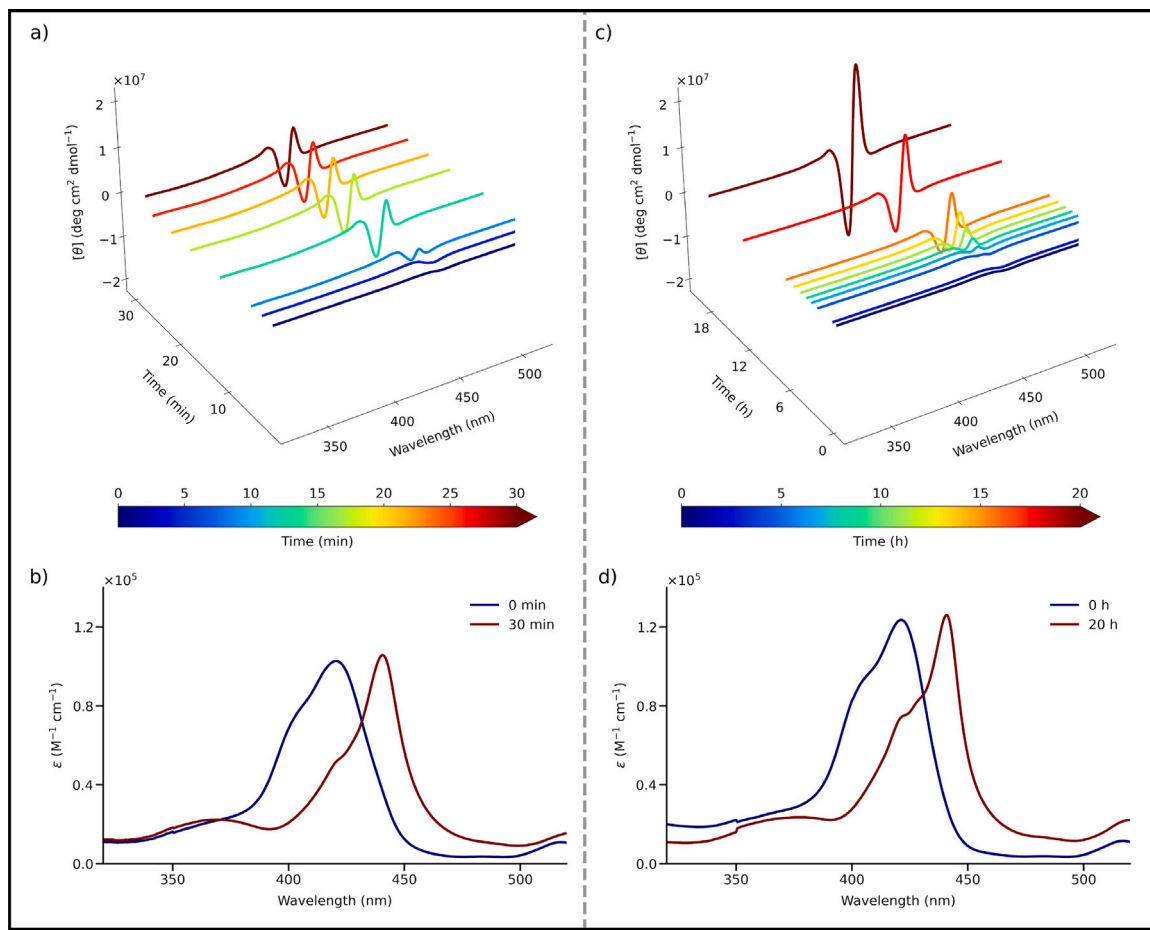


Fig. 4. (a) CD and (b) UV-Vis signal evolution with time for **1-H₂** at 30%_{vol} of acetonitrile; (c) CD and (d) UV-Vis signal evolution with time for **1-H₂** at 20%_{vol} of acetonitrile. The colour-bar, from blue to red, indicates the time, from the first moments of the aggregation to reaching the maximum growth at equilibrium.

Table 1

Kinetic data for the porphyrin-BS derivatives, in the solvent conditions of 7/3 and 8/2 of buffer/acetonitrile mixtures.

1-Zn	k_f (min ⁻¹)	n
buffer/ACN 7/3	$(1.6 \pm 0.3) \times 10^{-2}$	12 ± 1
buffer/ACN 8/2	$(1.2 \pm 0.2) \times 10^{-4}$	4 ± 2
1-H₂		
	k_f (min ⁻¹)	n
buffer/ACN 7/3	$(2.3 \pm 0.6) \times 10^{-1}$	5 ± 3
buffer/ACN 8/2	$(3.4 \pm 0.1) \times 10^{-3}$	2.0 ± 0.4

red-shifted of about 20 nm (440 nm), confirming the J-aggregates formation in solution (Fig. 4, b). However, the fast aggregation process leads to the formation of final architectures featuring a lower supramolecular order, as indicated by the corresponding CD spectrum (Fig. 4, a) of somewhat lower intensity, but always in the order of $10^7 \text{ deg cm}^2 \text{ dmol}^{-1}$. The evolution of the UV-Vis and CD spectra suggests that a much slower aggregate formation occurs at 20%_{vol} of acetonitrile, which is completed in about 20 h. For this sample, the CD is similar in shape to that obtained at 30%_{vol} of acetonitrile, but higher in intensity (Fig. 4, a and c). It is reasonable that the slower evolution is reflected in a more ordered supramolecular organization of the aggregates, with more specific interactions, according to the fundamental *reactivity vs specificity* principle. Also in this case, the UV-Vis spectrum resulted in a red-shift of the Soret band up to 440 nm (Fig. 4, d).

For **1-H₂** at 30%_{vol} of acetonitrile, the evolution of the Soret band was analysed by reporting the variation of the intensities at 420 and 440 nm, thereby revealing the progressive evolution of the spectral pattern (section 4 of SI, Fig. S4). On prolonged standing, a flocculation of some solid material occurred, likely due to further association and growth of the aggregated species.

Also for the free base porphyrin, a fit of the kinetic data was performed with Eq. (1). Formation constants and growth factors n of $(2.3 \pm 0.6) \times 10^{-1} \text{ min}^{-1}$ and 5 ± 3 , at acetonitrile 30%_{vol}, and of $(3.4 \pm 0.1) \times 10^{-3} \text{ min}^{-1}$ and 2.0 ± 0.4 , at acetonitrile 20%_{vol}, were obtained respectively.

It is worth noting that, for both the porphyrin-BS conjugates, a slight variation in the buffer/acetonitrile ratio (7/3 → 8/2) causes a lowering in the kinetic formation constant of the aggregates of two order of magnitude. On the contrary, considering the same solvent composition, the presence of the coordinated Zn(II) ion in the porphyrinic core has the effect of lowering k_f value by one order of magnitude for both the solvent mixtures (data reported in Table 1). However, the differences in the solvent composition affect the evolution kinetics of the aggregate formation, but not the supramolecular transmission of the chiral features, resulting, for both the molecules, in similar CD patterns.

3.2.3. DLS investigation

A DLS study of the hydrodynamic properties of these systems was generally hampered by the presence of large and sedimenting particles in solution. However, in the case of **1-H₂** in buffer/acetonitrile 7/3, that leads to constitute the aggregates after few minutes from the preparation, the first 30 min could be reliably followed by DLS. The

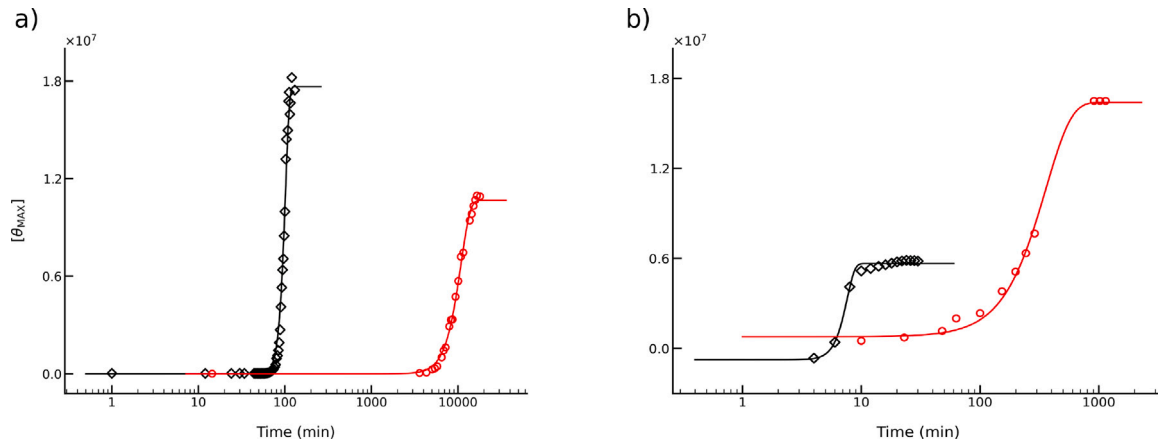


Fig. 5. Kinetic evolution of CD theta molar maxima ($[\theta_{MAX}]$ in $\text{deg cm}^2 \text{dmol}^{-1}$), for (a) **1-Zn** and (b) **1-H₂**, at acetonitrile 30%_{vol} (black diamonds) and 20%_{vol} (red circles). The solid lines, black and red respectively, describe the fitting of experimental data, according to Eq. (1). Porphyrins are in solution at 10 μM concentration. Time x-axis was reported in logarithmic scale.

time resolved analysis of the sizes of the aggregates was investigated reporting their relaxation times, τ , obtained from a non-negatively constrained least squares (NNLS) fitting algorithm. A sigmoidal trend was evidenced consistently with the sigmoidal evolution of CD and UV-Vis signals (section 11 of SI – Fig. S13 and Tab. S9). This result is a further confirmation of the auto-catalytic aggregation process.

Noteworthy, the initially formed Type-I species present τ values of about $3 \times 10^2 \mu\text{s}$, increasing to $\approx 4 \times 10^3 \mu\text{s}$, after 4–5 min, from the sample preparation, once the larger Type-II species are the predominant structures in solution.

3.3. Morphological studies of the chiral supramolecular architecture

To obtain a deep insight into the aggregates structure and to corroborate the spectroscopic results, a SEM and AFM microscopy investigation was performed on samples obtained after the completion of their kinetic evolution, in the different explored conditions. The SEM and AFM results coherently confirmed the presence of organized structures at the nano- or meso-scale, depending on the condition used, all presenting elongated morphologies, consistent with the UV-Vis excitonically coupled signal (see Section 3.2 and Refs. [89,96]).

More in detail, **1-Zn** samples showed the presence of helical ribbons along with less defined elongated structures at acetonitrile 30%_{vol} (Fig. 6, a – f). At acetonitrile 20%_{vol} the slower aggregation kinetics allowed the formation of more ordered supramolecular structures, providing tubules with monodisperse cross sections (Fig. 6, h – l). The two architecture, although found in different conditions, are probably different stages in the evolution of aggregates with the same supramolecular organization, considering that the formation of helical supramolecular ribbons is an intermediate stage in the commonly accepted mechanism of formation of tubules [97,98]. Cross section profiles, inferred from AFM images, show heights of about either 5–6 or 2–3 nm, randomly distributed among the structures for the sample at acetonitrile 30%_{vol} (Fig. 6, c – g). A height of 5–6 nm is instead homogeneously measured on the tubular aggregates obtained at acetonitrile 20%_{vol} (Fig. 6, i – l). Remarkably, the heights of 5–6 nm and the halved ones of 2–3 nm, regularly alternate along the helical ribbons at acetonitrile 30%_{vol} (Fig. 6, f – g, profile 2). Based on these findings a thickness of 2–3 nm is suggested for the ribbons and the wall of the tubules, which are supposed to lay flat on the mica surface. We anticipate that ribbons and tubule walls are formed by a bilayer of the derivatives comprising stacked porphyrin monomers with a possible ladder-like arrangement. A supramolecular organization is proposed,

implying as basilar unit a dimer with the aromatic macrocycles located inside, in a J-type head-tail configuration and the bile salt moieties located outside in opposite directions, in line with the structures obtained by quantum-mechanical geometry optimization (see Fig. S11 of section 10 in the supporting material). The dimension in length of the dimers constituting a bilayer was computed of around 5 nm, in accordance with the AFM cross section profiles, if considering a tilting in the angle, respect to the perpendicular, as shown in Fig. 7, b.

The organization of the free base porphyrin shows many interesting differences with respect to **1-Zn**, at both solvent compositions (Fig. 8), confirming the strong effect that the presence of the coordinated metal ion plays on the aggregation process. At 30%_{vol} of acetonitrile, again elongated structures are imaged in Fig. 8, a–f. Some details of the images (Fig. 8, e), show that the aggregates are formed by supramolecular sheets with a minimum height of about 4 nm wrapped into supramolecular rolls with tightly packed overlapped layers. The rolls extend in length for tens of microns. For these samples, heights in a wide range of values of about 20–55 nm are detected from the cross section profiles as expected for rolls of different thickness (number of overlapped layers). Also in this case, the value of measured minimum height (h_{min}) is comparable to the thickness of a double layer of free base porphyrins, as computed and reported in the supplementary information (data reported in section 10 of SI, figure S12).

Elongated structures are well visible also in the SEM images (see yellow arrows in Fig. 8, b). In these images, a side-by-side association of the primary elongated structures into secondary wider aggregates, with hundreds of nanometres width is observed. The width of the primary elongated structures estimated from the SEM images (Fig. 8, b and section 7 of supporting material) are in agreement with the height estimated from the cross section profiles of the AFM images (Fig. 8, g – i). Decreasing the amount of acetonitrile promotes a net morphological change in the free base porphyrin aggregates (Fig. 8, j – m). At a closer look, the flat structures shown in SEM image (Fig. 8, j) resemble the basilar sheets observed with a 30%_{vol} of acetonitrile (Fig. 8, a–b). These structures coexist with wrapped scrolls, with a hollow cavity inside, due to an apparent less tight winding (Fig. 8, k–m, showed by green arrows). The profile of image sections, showing heights of about 4 nm (suggested for the thickness of the single wall) and roughly the double value of about 8 nm (for the flat scroll obtained by the single winding of the scroll forming layer) supports the proposed structure. This is particularly evident from the profile 7 of Fig. 8, l where a jump from the height of one wall layer to twice this value highlights the partial winding of the wall forming layer. The AFM

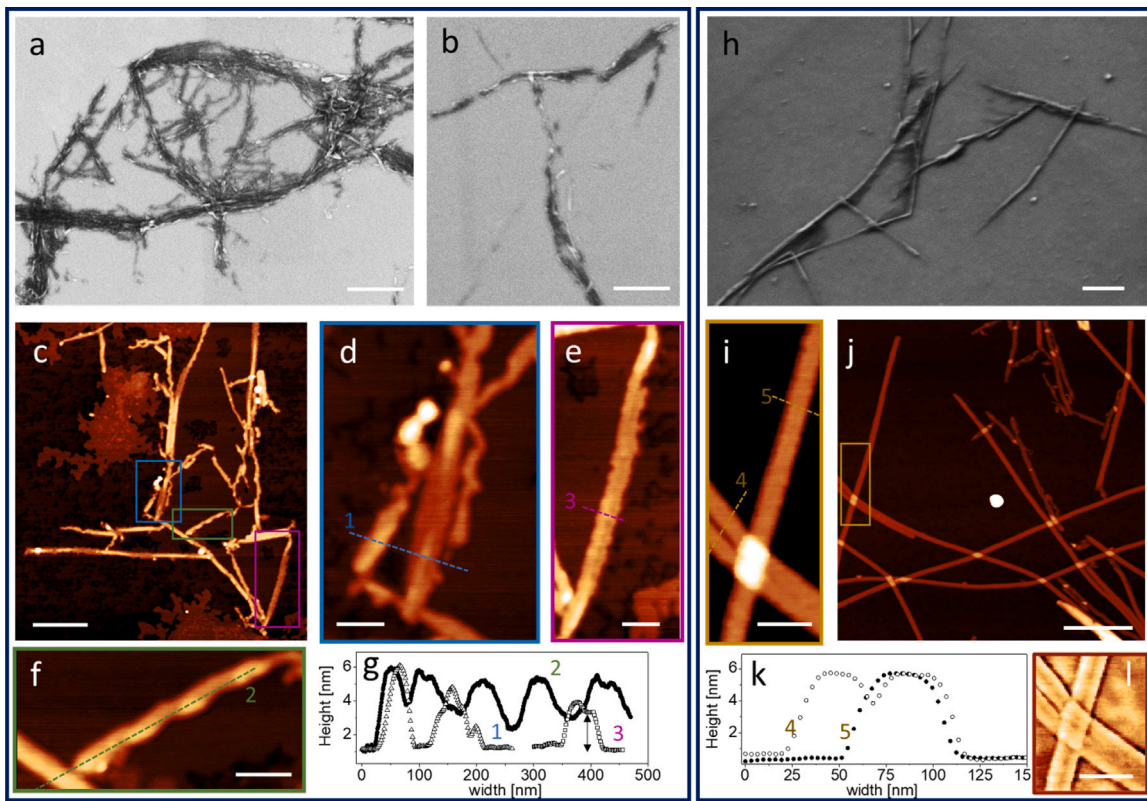


Fig. 6. SEM and AFM images of **1-Zn** at buffer/acetonitrile 7/3 (**a – b**, **c – f**) and in buffer/acetonitrile 8/2; (**h, i – l**). In **l** the image obtained by application of an horizontal Prewitt filter of a portion of AFM image **i** is shown. AFM height profiles are determined on the marked sections (**g – k**), with the minimum height attributable to a tilted bilayer size indicated by a double black arrow in profile **3** in **g**. Bar = 500 nm in **a, b, c, h, j**. Bar = 100 nm in **d, e, f, i, l**. From focus **f** a helical pitch of 100 ± 5 nm was estimated, as reported in the supporting material, section 12.

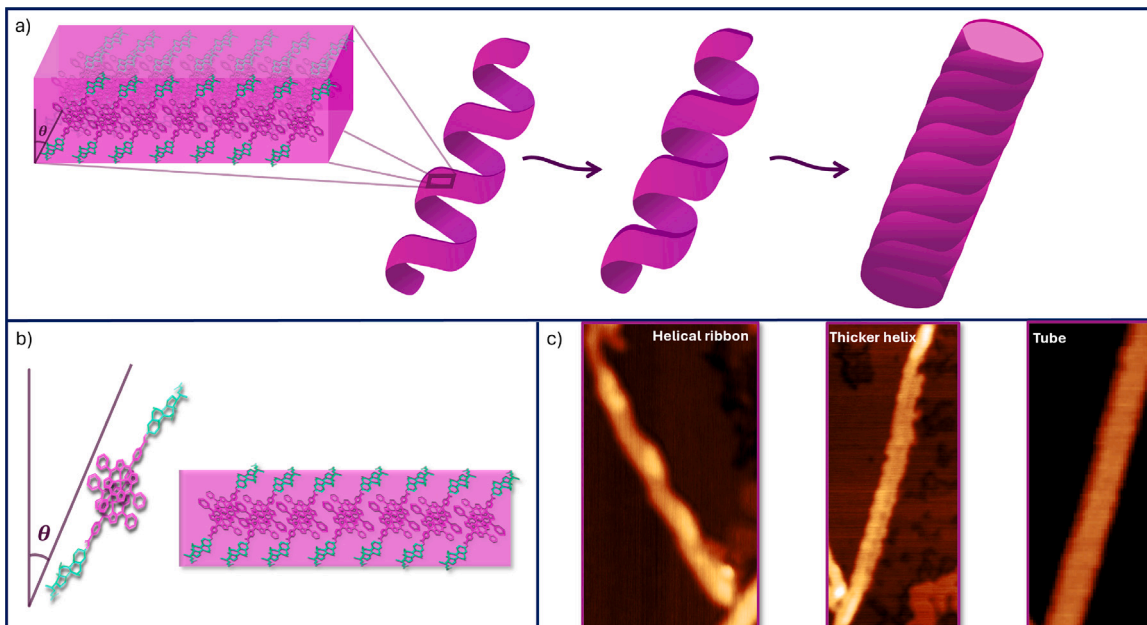


Fig. 7. (a) Graphical representation of the proposed aggregative mechanism for **1-Zn** molecule, from narrow helical ribbons to thicker helices, up to the formation of a tube. (b) Focus of the double layer. The porphyrin dimers constituting the double layer show a tilting angle, θ , respect to the perpendicular, that leads to a smaller width than that computed of around 5 nm. (c) AFM images reported as comparison (see Fig. 6, e-f-i).

profile traced on the evidence that the minimum height is again 3–4 nm (Fig. 8, l) and therefore compatible with the characteristic value of a bilayer. A more detailed analysis of the SEM widths and lengths is reported in section 7–8 of the supplementary material.

The analysis of the micrographs points out as a particularly important outcome that a flat fundamental structural motif with very similar thickness (between 2 and 4 nm) characterize the aggregates of both the porphyrins, in the two solvent conditions. This motif is

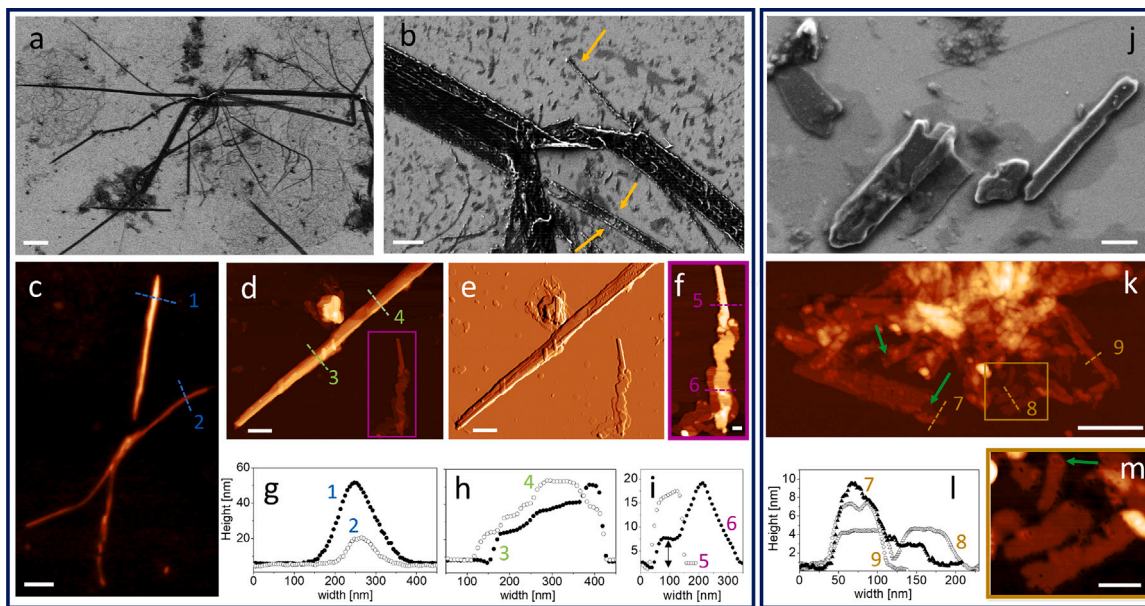


Fig. 8. SEM and AFM images of **1-H₂** in buffer/acetonitrile 7/3 (**a – b**, **c – f**) and in buffer/acetonitrile 8/2 (**j**, **k – m**). Note that focus **e** shows the horizontal Prewitt filtered image of focus **d**, for a better visualization of structural details. AFM height profile determined on the marked sections are shown in **g – i, l**, with the minimum height attributable to a tilted bilayer size indicated by a double black arrow in **i**, profile 5 (h_{\min} of 4.1 ± 0.2 nm). Bar = 5 μ m in panel **a–b**. Bar = 500 nm in **c – d – e – k**. Bar = 100 nm in **f – m**.

compatible with bilayer stacked macrocycles, if a tilt of the derivative is admitted to explain the slight differences in the computed and the measured thickness, as schematized in Fig. 7 for **1-Zn** samples, and easily extendable to the **1-H₂**. The presence of this fundamental motif in all samples is further supported by the similarity in the spectroscopic features highlighted by UV-Vis and CD described in Section 3.2.

4. Conclusion

In this study the synthesis and the aggregation behaviour of two new extrinsically chiral tetra-phenyl-porphyrin-BS conjugates have been investigated, by using both spectroscopic and microscopy techniques in combination. Mixtures of water and acetonitrile at different volume ratios were used to control the conjugates aggregation, by finely tuning the *solvophilic – solvophobic* balance of the system. Aimed at building nano- and meso-scopic systems featuring high supramolecular chirality, elongated aggregates with different structures like tubules or helical ribbons have been obtained depending on the solvent mixture, as well as the presence of a Zn(II) metal ion inside the porphyrinic core. Spectroscopic data demonstrated a J-type organization of the molecules in the aggregates. Time resolved spectroscopic measurements suggested a self-assembly kinetics comprising a fast monomer nucleation step followed by a slow second step of further growth and structuring of the supramolecular architectures. This is in agreement with the typical kinetics observed for related anionic proline-based amphiphilic porphyrin derivatives, studied in the recent past by some of our group [54,57].

Rod-like structures with variable degree of homogeneity were obtained for the metallated porphyrin (**1-Zn**). Instead, wrapped scrolls organized in tubular suprastructures were found for the free base (**1-H₂**) with a tight rolled packing, or with a looser arrangement that enables the formation of a cavity inside the tubes. The remarkable potentiality of hollow nanotubes is in providing a site of selective inclusion for a host-guest interaction [76] and the strong induction of supramolecular chirality may enable a specific chiral stereoselection.

The chance of easily tuning the structure of rod-like morphologies with tubular or rolled architectures, provides versatile systems for the preparation of elongated structures with different chiral compartments

able to enantioselectively accommodate chiral molecules. With the bile acid moiety acting as chiral effector [99], the more or less tight packing induced by the appropriate choice of the solvent mixture may offer suitable host sites for chiral guests of different size and chemical features. The general hydrophobicity of the porphyrin macrocycles – able to coordination and hydrogen bond interactions – can be thus translated in a more specific recognition [100,101].

In this context we foresee for our systems interesting potential for future applications in the ambit of stereoselective sensing materials and in particular for the design of quartz microbalance-based devices [10, 21, 22, 60, 102], with the possibility of a selective inclusion in a host-guest interaction [76] and, in general, in the wide field of soft matter for chiral and photonic applications [59, 100, 103–105].

CRediT authorship contribution statement

Valeria D'Annibale: Writing – review & editing, Writing – original draft, Visualization, Methodology, Investigation, Formal analysis, Data curation. **Luca Piccirillo:** Investigation, Formal analysis. **Beartrice Pacini:** Investigation, Formal analysis. **Simona Sennato:** Writing – review & editing, Visualization, Investigation, Data curation. **Claudia Marconi:** Methodology, Investigation. **Alessandra Del Giudice:** Writing – review & editing. **Maria Chiara di Gregorio:** Writing – review & editing, Investigation, Formal analysis. **Karin Schillén:** Writing – review & editing, Supervision, Investigation, Data curation. **Marco D'Abramo:** Writing – review & editing, Supervision, Investigation, Data curation. **Andrea D'Annibale:** Writing – review & editing, Writing – original draft, Supervision, Investigation, Data curation, Conceptualization. **Donato Monti:** Writing – review & editing, Writing – original draft, Supervision, Project administration, Investigation, Data curation, Conceptualization. **Luciano Galantini:** Writing – review & editing, Project administration, Conceptualization.

Declaration of competing interest

The authors declare that they have no known competing financial interests or personal relationships that could have appeared to influence the work reported in this paper.

Data availability

No data was used for the research described in the article.

Acknowledgements

Authors acknowledge CNIS – Research Center for Nanotechnology applied to Engineering of Sapienza, Sapienza University, Rome for access to AFM and SEM instrument.

Authors acknowledge Dr. Chiara Dal Bosco for the kind and precious help in performing LC-MS analysis.

M.C. di G. acknowledges support from the programme “Rita Levi Montalcini for young researchers” of the Italian Ministry of University and Research.

K.S. wishes to acknowledge the financial support of the Swedish Research Council (VR).

Appendix A. Supplementary data

Supplementary material related to this article can be found online at <https://doi.org/10.1016/j.colsurfa.2024.134507>.

References

- [1] D. Monti, Recent advancements in chiral porphyrin chemistry, *Top. Heterocycl. Chem.* 33 (2014) 231–292.
- [2] M.A. Castricano, A. Romeo, G. De Luca, V. Villari, L. Monsù-Scolaro, N. Micali, Scaling the chirality in Porphyrin J-nanoaggregates, *J. Am. Chem. Soc.* 133 (2011) 765–767.
- [3] R. Zanasi, P. Lazzeretti, A. Ligabue, A. Soncini, Theoretical results which strengthen the hypothesis of electroweak bioenantioselection, *Phys. Rev. E* 59 (1999) 3382–3385.
- [4] D.K. Kondepudi, G.W. Nelson, Chiral symmetry breaking in nonequilibrium systems, *Phys. Rev. Lett.* 50 (1983) 1023–1026.
- [5] D.K. Kondepudi, Selection of molecular chirality by extremely weak chiral interactions under far-from-equilibrium conditions, *Biosystems* 20 (1987) 75–83.
- [6] G. Zhang, X. Cheng, Y. Wang, W. Zhang, Supramolecular chiral polymeric aggregates: Construction and application, *Aggregate* 4 (2022) e262.
- [7] Y. Shen, Y. Wang, I.W. Hamley, W. Qi, R. Su, Z. He, Chiral self-assembly of peptides: Toward the design of supramolecular polymers with enhanced chemical and biological functions, *Prog. Polym. Sci.* 123 (2021) 101469.
- [8] J. Lv, X. Gao, B. Han, Y. Zhu, K. Hou, Z. Tang, Self-assembled inorganic chiral superstructures, *Nat. Rev. Chem.* 6 (2022) 125–145.
- [9] M. Stefanelli, R. Coticone, P. Sbardella, F. Ceccacci, G. Mancini, F. Mandoj, R. Paolesse, M. Venanzi, D. Monti, The aggregation of amphiphilic (L)-proline-porphyrin derivatives in ethanol-water mixtures promoted by chiral anionic surfactants, *J. Porphyr. Phthalocyanines* 21 (2017) 1–7.
- [10] E. Simoncini, F. Caroleo, F. Ceccacci, G. Mancini, M. Stefanelli, R. Paolesse, R. Lettieri, M. Venanzi, D. Monti, Chiral selectivity of Porphyrin-ZnO nanoparticle conjugates, *ACS Appl. Mater. Interfaces* 11 (2019) 12077–12087.
- [11] M. Stefanelli, F. Mandoj, G. Magna, R. Lettieri, M. Venanzi, R. Paolesse, D. Monti, The self-aggregation of Porphyrins with multiple chiral centers in organic/aqueous media: The case of sugar- and steroid-porphyrin conjugates, *Molecules* 25 (2020) 4544.
- [12] B. Brugnoli, A. Mariano, B. Simonis, C. Bombelli, S. Sennato, A. Piozzi, V. Taresco, V.M. Chauhan, S.M. Howdle, A. Scotti d'Abusco, I. Francolini, Self-assembled chitosan-sodium usnate drug delivery nanosystems: Synthesis, characterization, stability studies, in vitro cytotoxicity and in vivo biocompatibility against 143 B cells, *Carbohydr. Polym. Technol. Appl.* 6 (2023) 100373.
- [13] G. El-Hachemi, Mancini, J.M. Ribó, A. Sorrenti, Role of the hydrophobic effect in the transfer of chirality from molecules to complex systems: From chiral surfactants to porphyrin/surfactant aggregates, *J. Am. Chem. Soc.* 130 (2008) 15176–15184.
- [14] P. Dognini, C.R. Coxon, W.A. Alves, F. Giuntini, Peptide-tetrapyrrole supramolecular self-assemblies: State of the art, *Molecules* 26 (3) (2021).
- [15] R. Oda, I. Huc, M. Schmutz, S.J. Candalu, F.C. MacKintosh, Tuning bilayer twist using chiral counterions, *Nature* 399 (1999) 566–569.
- [16] A. Tonizzo, M. Cerminara, G. Macchi, N. Periasamy, P. Sozzani, R. Tubino, Optical excitations of porphyrin J-aggregates, *Synth. Met.* 155 (2005) 291–294.
- [17] S.L. Thorpe, G.N. Snyder, A. Mammana, Spectroscopic study of porphyrin self-assembly: Role of pH, time and chiral template, *Chirality* 32 (2020) 5–16.
- [18] J. Tian, W. Zhang, Synthesis, self-assembly and applications of functional polymers based on porphyrins, *Prog. Polym. Sci.* 95 (2019) 65–117.
- [19] C. Zhang, P. Chen, H. Dong, Y. Zhen, M. Liu, W. Hu, Porphyrin supramolecular 1D structures via surfactant-assisted self-assembly, *Adv. Mater.* 27 (2015) 5379–5387.
- [20] H. Jintoku, M. Takafuji, R. Oda, H. Ihara, Enantioselective recognition by a highly ordered porphyrin-assembly on a chiral molecular gel, *Chem. Commun.* 48 (2012) 4881–4883.
- [21] R. Paolesse, S. Nardis, D. Monti, M. Stefanelli, C. Di Natale, Porphyrinoid for chemical sensor applications, *Chem. Rev.* 117 (2017) 2517–2583.
- [22] G. Magna, M. Šákarová, M. Stefanelli, G. Giancane, S. Bettini, L. Valli, L. Ustrnul, V. Borovkov, R. Aav, D. Monti, C. Di Natale, R. Paolesse, Chiral recognition by supramolecular Porphyrin-Hemicucurbit[8]uril-functionalized gravimetric sensors, *ACS Appl. Mater. Interfaces* 15 (2023) 30674–30683.
- [23] S. Matile, N. Berova, K. Nakanishi, S. Novkova, I. Philipova, B. Blagoev, Porphyrins: Powerful chromophores for structural studies by exciton-coupled circular dichroism, *J. Am. Chem. Soc.* 117 (1995) 7021–7022.
- [24] S. Matile, N. Berova, K. Nakanishi, J. Fleischhauer, R.W. Woody, Structural studies by exciton coupled circular dichroism over a large distance: Porphyrin derivatives of steroids, dimeric steroids, and brevetoxin B, *J. Am. Chem. Soc.* 118 (1996) 5198–5206.
- [25] G. Pescitelli, S. Gabriel, Y. Wang, J. Fleischhauer, R.W. Woody, N. Berova, Theoretical analysis of the Porphyrin-Porphyrin exciton interaction in circular dichroism spectra of dimeric tetraarylporphyrins, *J. Am. Chem. Soc.* 125 (2003) 7613–7628.
- [26] F. Wurthner, T.E. Kaiser, C.R. Saha-Möller, J-aggregates: From serendipitous discovery to supramolecular engineering of functional dye materials, *Angew. Chem. Int. Edn* 50 (2011) 3376–3410.
- [27] E. Jolley, Spectral absorption and fluorescence of dyes in the molecular state, *Nature* 138 (1936) 1009–1010.
- [28] V. Villari, P. Mineo, E. Scamporrino, N. Micali, Role of the hydrogen-bond in porphyrin J-aggregates, *RCS Adv.* 2 (2012) 12989–12998.
- [29] E. Simoncini, F. Caroleo, F. Ceccacci, G. Mancini, M. Stefanelli, R. Paolesse, R. Lettieri, M. Venanzi, D. Monti, Surfactant-induced chirality on reluctant aggregates of a chiral amphiphilic cationic (L)-proline-Zn(II)porphyrin conjugate in water, *RSC Adv.* 4 (2014) 55362–55366.
- [30] A. Alzalamira, F. Ceccacci, D. Monti, S. Levi Mortera, G. Mancini, A. Sorrenti, M. Venanzi, C. Villani, Discrimination of the enantiomers of biphenylidic derivatives in micellar aggregates formed by chiral amide surfactants, *Asymmetry* 18 (2007) 1868–1876.
- [31] L. Duan, C. Wang, W. Zhang, B. Ma, Y. Deng, W. Li, D. Zhao, Interfacial assembly and applications of functional mesoporous materials, *Chem. Rev.* 121 (2021) 14349–14429.
- [32] A. Escudero, C. Carrillo-Carrión, M.C. Castillejos, E. Romero-Ben, C. Rosales-Barrios, N. Khiar, Photodynamic therapy: Photosensitizers and nanostructures, *Mater. Chem. Front.* 5 (2021) 3788–3812.
- [33] T.J. Dougherty, C.J. Gomer, B.W. Henderson, G. Jori, D. Kessel, M. Korbelik, J. Moan, Q. Peng, Photodynamic therapy, *JNCI* 90 (1998) 889–905.
- [34] B.M. Amos-Tautu, S.P. Songca, O.S. Oluwafemi, Application of Porphyrins in antibacterial photodynamic therapy, *Molecules* 24 (13) (2019).
- [35] Y. Liu, R. Qin, S.A.J. Zaat, E. Breukink, M. Heger, Antibacterial photodynamic therapy: Overview of a promising approach to fight antibiotic-resistant bacterial infections, *J. Clin. Transl. Res.* 1 (2015) 140–167.
- [36] M.L. Sagristá, F. Postigo, M.A. De Madariaga, R.M. Pintoó, S. Caballero, A. Bosch, M.A. Vallé, M. Mora, Photodynamic inactivation of viruses by immobilized chlorin-containing liposomes, *J. Porphyrins Phthalocyanines* 13 (2008) 578–588.
- [37] J. Cautela, E. Severoni, C. Redondo-Gómez, M.C. di Gregorio, A. Del Giudice, S. Sennato, R. Angelini, M. D'Abramo, K. Schillén, L. Galantini, C-12 vs C-3 substituted bile salts: An example of the effects of substituent position and orientation on the self-assembly of steroid surfactant isomers, *Colloids Surf. B* 185 (2020) 110556.
- [38] M.C. di Gregorio, L. Travaglini, A. Del Giudice, J. Cautela, N.V. Pavel, L. Galantini, Bile salts: Natural surfactants and precursors of a broad family of complex amphiphiles, *Langmuir* 35 (2019) 6803–6821.
- [39] M.C. di Gregorio, J. Cautela, L. Galantini, Physiology and physical chemistry of bile acids, *Int. J. Mol. Sci.* 22 (2021) 1780.
- [40] G. Du, D. Belić, A. Del Giudice, V.A. Alfredsson, A.M. Carnerup, K. Zhu, B. Nyström, Y. Wang, L. Galantini, K. Schillén, Condensed supramolecular Helices: The twisted sisters of DNA, *Angew. Chem. Int. Edn* 61 (2022) e202113279.
- [41] A. Jover, F. Fraga, F. Mejide, J. Vázquez Tato, J. Cautela, A. Del Giudice, M.C. di Gregorio, Revealing the complex self-assembly behaviour of sodium deoxycholate in aqueous solution, *J. Colloid Interface Sci.* 604 (2021) 415–428.
- [42] V.H.S. Tellini, A. Jover, F. Mejide, J.V. Tato, L. Galantini, N.V. Pavel, Supramolecular structures generated by a *p-tert*-butylphenylamide derivative of cholic acid: From vesicles to molecular tubes, *Adv. Mater.* 19 (2007) 1752–1756.
- [43] L. Galantini, C. Leggio, A. Jover, F. Mejide, N.V. Pavel, V.H.S. Tellini, J.V. Tato, R. Di Leonardo, G. Ruocco, Kinetics of formation of supramolecular tubules of a sodium cholate derivative, *Soft Matter* 5 (2009) 3018–3025.
- [44] L. Zhang, Y. Fan, L. Galantini, K. Schillén, A. Del Giudice, G. Du, Y. Wang, Noncovalent bile acid oligomers as facial amphiphilic antimicrobials, *Langmuir* 39 (2023) 495–506.

- [45] M. Di Consiglio, E. Sturabotti, B. Brugnoli, A. Piozzi, L. Migneco, I. Francolini, Synthesis of sustainable eugenol/hydroxyethylmethacrylate-based polymers with antioxidant and antimicrobial properties, *Polym. Chem.* 14 (2023) 432.
- [46] C. Lin, Y. Wang, M. Le, K.-F. Chen, Y.-G. Jia, Recent progress in bile acid-based antimicrobials, *Bioconjug. Chem.* 32 (3) (2021) 395–410.
- [47] E. Zarenehad, M. Marzi, H.T. Abdulabbas, S.A. Jasim, S.A. Kouhpayeh, S. Barbaresi, S. Ahmadi, A. Ghasemian, Bilosomes as nanocarriers for the drug and vaccine delivery against gastrointestinal infections: Opportunities and challenges, *J. Funct. Biomater.* 14 (2023) 453.
- [48] L. Travaglini, A. D'Annibale, K. Schillén, U. Olsson, S. Sennato, N.V. Pavel, L. Galantini, Amino acid-bile acid based molecules: Extremely narrow surfactant nanotubes formed by a phenylalanine-substituted cholic acid, *Chem. Commun.* 48 (2012) 12011–12013.
- [49] L. Travaglini, M. Gubitosi, M.C. di Gregorio, N.V. Pavel, A. D'Annibale, M. Giustini, V.H.S. Tellini, J.V. Tato, M. Obiols-Rabasa, S. Bayati, L. Galantini, On the self-assembly of a tryptophan labeled deoxycholic acid, *Phys. Chem. Chem. Phys.* 16 (2014) 19492–19504.
- [50] M. Gubitosi, F. Meijide, A. D'Annibale, J.V. Tato, A. Jover, L. Galantini, L. Travaglini, M.C. di Gregorio, N.V. Pavel, Crystal structure of a lithium salt of a glucosyl derivative of lithocholic acid, *Steroids* 113 (2016) 87–94.
- [51] L. Galantini, M.C. di Gregorio, M. Gubitosi, L. Travaglini, J.V. Tato, A. Jover, F. Meijide, V.H.S. Tellini, N.V. Pavel, Bile salts and derivatives: Rigid unconventional amphiphiles as dispersants, carriers and superstructure building blocks, *Curr. Opin. Colloid Interface Sci.* 20 (2015) 170–182.
- [52] J.V. Trillo, F. Meijide, A. Jover, V.H.S. Tellini, S. de Frutos, M.C. di Gregorio, L. Galantini, J.V. Tato, Self-aggregation mechanism of a naphthylamide cationic derivative of cholic acid. From fibers to tubules, *RSC Adv.* 4 (2014) 5598.
- [53] J. Cautela, B. Stenqvist, K. Schillén, D. Belić, L.K. Månnsson, F. Hagemanns, M. Seuss, A. Fery, J.J. Crassous, L. Galantini, Supracolloidal atomium, *ACS Nano* 14 (2020) 15748–15756.
- [54] M. Savioli, M. Stefanelli, G. Magna, F. Zurlo, M.F. Caso, R. Cimino, C. Goletti, M. Venanzi, C. Di Natale, R. Paolesse, D. Monti, Tunable supramolecular chirogenesis of amphiphilic Porphyrin triggered by chiral amines, *Int. J. Mol. Sci.* 21 (2020) 8557.
- [55] Z. El-Hachemi, C. Escudero, O. Arteaga, A. Canillas, J. Crusats, G. Mancini, R. Purrello, A. Sorrenti, A. D'Urso, J.M. Ribó, Chiral sign selection on the J-aggregates of diprotонated tetrakis-(4-sulfonatophenyl)porphyrin by traces of unidentified chiral contaminants present in the ultra-pure water used as solvent, *Chirality* 21 (2009) 408–412.
- [56] D. Monti, M. Stefanelli, M. Raggio, N. Colozza, M. Venanzi, R. Lettieri, L. Luvidi, G. Laguzzi, S. Bonacchi, D. Weber, L. Prodi, C. Di Natale, R. Paolesse, Solid state deposition of chiral amphiphilic porphyrin derivatives on glass surface, *J. Porphyr. Phthalocyanines* 15 (2011) 1209–1219.
- [57] M. Stefanelli, M. Savioli, F. Zurlo, G. Magna, S. Belviso, G. Marsico, S. Superchi, M. Venanzi, C. Di Natale, R. Paolesse, D. Monti, Porphyrins through the looking glass: Spectroscopic and mechanistic insights in supramolecular chirogenesis of new self-assembled porphyrin derivatives, *Front. Chem.* 8 (2020) 587842.
- [58] F. Caroleo, M. Stefanelli, G. Magna, M. Venanzi, R. Paolesse, S. Sennato, M. Carbonne, D. Monti, Kinetic and spectroscopic studies on the chiral self-aggregation of amphiphilic zinc and copper (L)-proline-tetraarylporphyrin derivatives in different aqueous media, *Org. Biomol. Chem.* 17 (2019) 1113–1120.
- [59] G. Magna, T. Traini, M.L. Naitana, G. Bussetti, F. Domenici, G. Paradossi, M. Venanzi, C. Di Natale, P. Roberto, D. Monti, M. Stefanelli, Seeding chiral ensembles of prolinated Porphyrin derivatives on glass surface: Simple and rapid access to chiral Porphyrin films, *Front. Chem.* 9 (2022) 804893.
- [60] M. Stefanelli, G. Magna, C. Di Natale, R. Paolesse, D. Monti, Stereospecific self-assembly process of Porphyrin-proline conjugates: From the effect of structural features and bulk solvent properties to the application in stereoselective sensor systems, *Mol. Sci.* 23 (2022) 15587.
- [61] C. Di Natale, R. Paolesse, A. Macagnano, A. Mantini, C. Goletti, A. D'Amico, Characterization and design of porphyrins-based broad selectivity chemical sensors for electronic nose applications, *Sens. Actuators B Chem.* 52 (1998) 162–168.
- [62] D. Monti, M. Venanzi, E. Gatto, G. Mancini, A. Sorrenti, P. Štěpánek, P. Drašar, Study of the supramolecular chiral assembly of meso-C-glucoside-porphyrin derivatives in aqueous media, *New. J. Chem.* 32 (2008) 2127–2133.
- [63] R. Lettieri, D. Monti, K. Zelenka, T. Trnka, P. Drašar, M. Venanzi, Glucosylated steroid-porphyrins as new tools for nanotechnology applications, *New J. Chem.* 36 (2012) 1246–1254.
- [64] K. Zelenka, T. Trnka, I. Tišlerová, D. Monti, S. Cinti, M.L. Naitana, L. Schiaffino, M. Venanzi, G. Laguzzi, L. Luvidi, G. Mancini, Z. Nováková, O. Šimák, Z. Wimmer, P. Drašar, Spectroscopic, morphological, and mechanistic investigation of the solvent-promoted aggregation of porphyrins modified in meso-positions by glucosylated steroids, *Chem. Eur. J.* 17 (2011) 13743–13753.
- [65] M.L. Naitana, M. Dukh, K. Zelenka, T. Trnka, M. Venanzi, R. Lettieri, P. Drašar, D. Monti, The kinetic studies of the solvent-promoted aggregation of a steroid-porphyrin derivative, *J. Porphyr. Phthalocyanines* 17 (2013) 889–895.
- [66] X. Huang, K. Nakanishi, N. Berova, Porphyrins and metalloporphyrins: Versatile circular dichroic reporter groups for structural studies, *Chirality* 12 (2000) 237–255.
- [67] T. Ishi-i, J.H. Jung, S. Shinkai, Intermolecular porphyrin-fulleren interaction can reinforce the organogel structure of a porphyrin-appended cholesterol derivative, *J. Mater. Chem.* 10 (2000) 2238–2240.
- [68] T. Ishi-i, R. Iguchi, E. Snip, M. Ikeda, S. Shinkai, [60]Fullerene can reinforce the organogel structure of porphyrin-appended cholesterol derivatives: Novel odd-even effect of the $(\text{CH}_2)_n$ spacer on the organogel stability, *Langmuir* 17 (2001) 5825–5833.
- [69] R. Fong II, D.I. Schuster, S.R. Wilson, Synthesis and photophysical properties of steroid-linked porphyrin-fullerene hybrids, *Org. Lett.* 1 (1999) 729–732.
- [70] E. Gireggi, R. Ricoux, J.-P. Mahy, Design and synthesis of a Mn(III)-porphyrin steroid conjugate used as a new cleavable affinity label: On the road to semi-synthetic catalytic antibodies, *Tetrahedron* 60 (2004) 10049–10058.
- [71] S. Tomas, L. Milanesi, Hydrophobically self-assembled nanoparticles as molecular receptors in water, *J. Am. Chem. Soc.* 131 (2009) 6618–6623.
- [72] H.A. Zhylitskaya, V.N. Zhabinskii, R.P. Litvinovskaya, R. Lettieri, D. Monti, M. Venanzi, V.A. Khrapach, P. Drasar, Design and studies of novel polyoxysterol-based porphyrin conjugates, *Steroids* 77 (2012) 1169–1175.
- [73] C. Lorecchio, M. Venanzi, C. Mazzuca, R. Lettieri, A. Palleschi, T.H. Nguyen Thi, L. Cardová, P. Drasar, D. Monti, Tuning the chiroptical and morphological properties of steroid-porphyrin aggregates: A mechanistic, structural, and MM investigation, *Org. Biomol. Chem.* 12 (2014) 3956–3963.
- [74] Q. Zou, M. Abbas, L. Zhao, S. Li, G. Shen, X. Yan, Biological photothermal nanodots based on self-assembly of peptide-porphyrin conjugates for antitumor therapy, *J. Am. Chem. Soc.* 139 (2017) 1921–1927.
- [75] S. Jenni, G. Picci, M. Fornasier, M. Mamusa, J. Schmidt, Y. Talmon, A. Sour, V. Heitz, S. Murgia, C. Caltagirone, Multifunctional cubic liquid crystalline nanoparticles for chemo- and photodynamic synergistic cancer therapy, *Photochem. Photobiol. Sci.* 19 (2020) 674–680.
- [76] D.D. La, T.D. Dang, P.C. Le, X.T. Bui, S.W. Chang, W.J. Chung, S.C. Kim, D.D. Nguyen, Self-assembly of monomeric porphyrin molecules into nanostructures: Self-assembly pathways and applications for sensing and environmental treatment, *Environ. Technol. Innov.* 29 (2023) 103019.
- [77] M. Younis, S. Ahmad, A. Atiq, M.A. Farooq, M. Huang, M. Abbas, Recent progress in Azobenzene-based supramolecular materials and applications, *Chem. Rec.* 23 (2023) e2023001.
- [78] X. Zou, C. Liu, C. Li, R. Fu, W. Xu, H. Bian, X. Dong, X. Zhao, Z. Xu, J. Zhang, Z. Shen, Study on the structure-activity relationship of dihydroartemisinin derivatives: Discovery, synthesis, and biological evaluation of dihydroartemisinin-bile acid conjugates as potential anticancer agents, *Eur. J. Med. Chem.* 225 (2021) 113754.
- [79] V.S. Pore, N.G. Aher, M. Kumar, P.K. Shukla, Design and synthesis of fluconazole/bile acid conjugate using click reaction, *Tetrahedron* 62 (48) (2006) 11178–11186.
- [80] D.B. Salunke, D.S. Ravi, V.S. Pore, D. Mitra, B.G. Hazra, Amino functionalized novel cholic acid derivatives induce HIV-1 replication and syncytia formation in T cells, *J. Med. Chem.* 49 (2006) 2652–2655.
- [81] D. Monti, M. De Rossi, A. Sorrenti, G. Laguzzi, E. Gatto, M. Stefanelli, M. Venanzi, L. Luvidi, M. Mancini, R. Paolesse, Supramolecular chirality in solvent-promoted aggregation of amphiphilic porphyrin derivatives: Kinetic studies and comparison between solution behavior and solid-state morphology by AFM topography, *Chem. Eur. J.* 16 (2010) 860–870.
- [82] M. Liu, L. Zhang, T. Wang, Supramolecular chirality in self-assembled systems, *Chem. Rev.* 115 (2015) 7304–7397.
- [83] J.-D. Chai, M. Head-Gordon, Long-range corrected hybrid density functionals with damped atom-atom dispersion corrections, *Phys. Chem. Chem. Phys.* 10 (2008) 6615–6620.
- [84] J. Tomasi, R. Bonaccorsi, R. Cammi, F. Olivares del Valle, Theoretical chemistry in solution. Some results and perspectives of the continuum methods and in particular of the polarizable continuum model, *J. Mol. Struct.* 234 (1991) 401–424.
- [85] M.J. Frisch, G.W. Trucks, H.B. Schlegel, G.E. Scuseria, M.A. Robb, J.R. Cheeseman, G. Scalmani, V. Barone, G.A. Petersson, H. Nakatsuji, X. Li, M. Caricato, A.V. Marenich, J. Bloino, B.G. Janesko, R. Gomperts, B. Mennucci, H.P. Hratchian, J.V. Ortiz, A.F. Izmaylov, J.L. Sonnenberg, D. Williams-Young, F. Ding, F. Lipparini, F. Egidi, J. Goings, B. Peng, A. Petrone, T. Henderson, D. Ranasinghe, V.G. Zakrzewski, J. Gao, N. Rega, G. Zheng, W. Liang, M. Hada, M. Ehara, K. Toyota, R. Fukuda, J. Hasegawa, M. Ishida, T. Nakajima, Y. Honda, O. Kitao, H. Nakai, T. Vreven, K. Throssell, J.A. Montgomery Jr., J.E. Peralta, F. Ogliaro, M.J. Bearpark, J.J. Heyd, E.N. Brothers, K.N. Kudin, V.N. Staroverov, T.A. Keith, R. Kobayashi, J. Normand, K. Raghavachari, A.P. Rendell, J.C. Burant, S.S. Iyengar, J. Tomasi, M. Cossi, J.M. Millam, M. Klene, C. Adamo, R. Cammi, J.W. Ochterski, R.L. Martin, K. Morokuma, O. Farkas, J.B. Foresman, D.J. Fox, Gaussian16 revision c.01, 2016, Gaussian Inc. Wallingford CT.
- [86] R.F. Pasternack, C. Fleming, S. Herring, P.J. Collings, J. dePaula, G. DeCastro, E.J. Gibbs, Aggregation kinetics of extended porphyrin and cyanine dye assemblies, *Biophys. J.* 79 (2000) 550–560.
- [87] R.F. Pasternack, E.J. Gibbs, D. Bruzewicz, D. Stewart, K.S. Engstrom, Kinetics of disassembly of a DNA-bound porphyrin supramolecular array, *J. Am. Chem. Soc.* 124 (2002) 3533–3539.

- [88] N. Micali, A. Romeo, R. Lauceri, R. Purrello, F. Mallamace, L. Mosù Scolaro, Fractal structures in homo- and heteroaggregated water soluble porphyrins, *J. Phys. Chem. B* 104 (2000) 9416–9420.
- [89] J.M. Short, J.A. Berriman, C. Kubel, Z. El-Hachemi, J.-V. Naubron, T.S. Balaban, Electron cryo-microscopy of TPPS₄× 2HCl tubes reveals a helical organisation explaining the origin of their chirality, *ChemPhysChem* 14 (2013) 3209–3214.
- [90] V. Gutmann, Solvent effects on the reactivities of organometallic compounds, *Coord. Chem. Rev.* 18 (1976) 225–255.
- [91] R. Miranda-Quintana, J. Smiatek, Calculation of donor numbers: Computational estimates for Lewis basicity solvents, *J. Mol. Liq.* 322 (2021) 114506.
- [92] R. Schmid, Re-interpretation of the solvent dielectric constant in coordination chemical terms, *J. Solution Chem.* 12 (1983) 135–152.
- [93] P. Štěánek, M. Dukh, D. Šaman, J. Moravcová, L. Kniežo, D. Monti, M. Venanzi, G. Mancini, P. Drašar, Synthesis and solvent driven self-aggregation studies of meso-“c-glycoside”-porphyrin derivatives, *Org. Biomol. Chem.* 5 (2007) 960–970.
- [94] M.C. di Gregorio, M. Varenik, M. Gubitosi, L. Travaglini, N.V. Pavel, A. Jover, F. Meijide, O. Regev, L. Galantini, Multi stimuli response of a single surfactant presenting a rich self-assembly behavior, *RSC Adv.* 5 (2015) 37800.
- [95] A. Sorrenti, Z. El-Hachemi, O. Arteaga, A. Canillas, J. Crusats, J.M. Ribò, Kinetic control of the supramolecular chirality of J-aggregates, *Chem. Eur. J.* 18 (2012) 8820–8826.
- [96] O. Ohno, Y. Kaizu, H. Kobayashi, J-aggregate formation of a water-soluble porphyrin in acidic aqueous media, *J. Chem. Phys.* 99 (1993) 4128–4139.
- [97] J.V. Selinger, M.S. Spector, J.M. Schnur, Theory of self-assembled tubules and helical ribbons, *J. Phys. Chem. B* 105 (2001) 7157–7169.
- [98] L. Ziserman, H.-Y. Lee, S. Raghavan, A. Mor, D. Danino, Unraveling the mechanism of nanotube formation by chiral self-assembly of amphiphiles, *J. Am. Chem. Soc.* 133 (2011) 2511–2517.
- [99] S. Patel, D. Bariya, R. Mishra, S. Mishra, Bile acid-based receptors and their applications in recognition, *Steroids* 179 (2022) 108981.
- [100] L. Zhang, T. Wang, J. Jiang, M. Liu, Chiral porphyrin assemblies, *Aggregate* 4 (2023) e198.
- [101] C. Oliveras-González, F. Di Meo, A. González-Campo, D. Beljonne, P. Norman, M. Simón-Sorbed, M. Linares, D. Amabilino, Bottom-up hierarchical self-assembly of chiral porphyrins through coordination and hydrogen bonds, *J. Am. Chem. Soc.* 137 (2015) 15795–15808.
- [102] Z. Anfar, B. Kuppan, A. Scalabre, R. Nag, E. Pouget, S. Nlate, G. Magna, I. Di Filippo, D. Monti, M.L. Naitana, M. Stefanelli, T. Nikonorich, V. Borovkov, R. Aav, R. Paolesse, R. Oda, Porphyrin-based hybrid nanohelices: Cooperative effect between molecular and supramolecular chirality on amplified optical activity, *J. Phys. Chem. B* 128 (2024) 1550–1556.
- [103] A. Scalabre, Y. Okazaki, B. Kuppan, T. Buffeteau, F. Caroleo, G. Magna, D. Monti, R. Paolesse, M. Stefanelli, S. Nlate, E. Pouget, H. Ihara, D.M. Bassani, Chirality induction to achiral molecules by silica-coated chiral molecular assemblies, *Chirality* 33 (2021) 494–505.
- [104] G. Giancane, R. Pagano, M. Naitana, G. Magna, M. Stefanelli, D. Monti, R. Paolesse, S. Bettini, L. Valli, Proline enantiomers discrimination by (L)-prolineated Porphyrin derivative Langmuir-Schaefer films: Proof of concept for chiral sensing applications, *Chemosensors* 10 (2022) 331.
- [105] D.G. Baranov, C. Schäfer, M.V. Gorkunov, Toward molecular chiral polaritons, *ACS Photonics* 10 (2023) 2440–2455.